

Tunable blue-green emission from ZnS(Ag) nanostructures grown by hydrothermal synthesis

Manjula Sharma

Technical Physics Division, Bhabha Atomic Research Center, Trombay, Mumbai 400085, India; and Department of Physics and Astrophysics, University of Delhi, New Delhi 110007, India

Shashwati Sen,^{a)} Jagannath Gupta, M. Ghosh, and S. Pitale

Technical Physics Division, Bhabha Atomic Research Center, Trombay, Mumbai 400085, India

Vinay Gupta

Department of Physics and Astrophysics, University of Delhi, New Delhi 110007, India

S.C. Gadkari

Technical Physics Division, Bhabha Atomic Research Center, Trombay, Mumbai 400085, India

(Received 26 April 2018; accepted 10 September 2018)

We report the synthesis and optical properties of pure ZnS and Ag doped ZnS nanostructures. ZnS(Ag) was synthesized by using the hydrothermal technique and later annealed at different temperatures under vacuum conditions. It was observed that the photoluminescence (PL) emission from the ZnS(Ag) nanostructures can be easily tuned from the blue (445 nm) to green (530 nm) region of visible light by varying the annealing temperature. This tunability has been attributed to the introduction of excess sulfur vacancy states, which is evident from the PL excitation spectra. This observed change in the PL emission wavelength can be highly beneficial in the imaging screens where ZnS is regularly used and can be easily interfaced with the silicon photodiodes showing maximum sensitivity at 550 nm.

I. INTRODUCTION

ZnS is a significant II–VI wide band-gap semiconductor material which has attracted a lot of interest due to its potential applications in various fields. It is a very important material for electronic industry with its usage ranging from efficient phosphors in flat panel displays, light-emitting diodes, and field emitters to UV light sensors, gas sensors,¹ photovoltaics, photo catalysis,^{2,3} etc. ZnS nanostructures in the form of micro/nanobelts having large surface area are suitable for UV detectors.⁴ Also, ZnS exhibits a high exciton binding energy at room temperature which makes it further favorable candidate for light-emission based devices.⁵

ZnS has two structural polymorphs, the cubic zinc blende structure and hexagonal wurtzite structure having band-gaps of 3.72 eV and 3.77 eV, respectively, at room temperature. Quantum confinement in the synthesized ZnS nanoparticles has led to further improvement in their properties.⁶ It has been demonstrated by various groups that by controlling the structure and size of the ZnS nanoparticles, its properties can be tuned according to the required applications.^{7,8}

It is well known that pure ZnS emits at around 420 nm which is termed as self-activated emission.⁶ The

luminescence properties of ZnS have been a hot topic of research and are reported to be highly tuned by external elements. Interstitial defects and vacancies also play an important role by forming intermediate energy levels in ZnS which act as luminescent centers. Donor levels are formed by the sulfur vacancies and zinc interstitials present in ZnS, whereas Zn vacancies and S interstitials form acceptor levels.⁹ Generally, the luminescence from ZnS is related to the sulfur and zinc vacancies or to the elemental sulfur species forming the surface states. The impurity states present in the material in the form of heavy-atom doping also contribute to the high luminescence yield. Thus, the interesting properties of ZnS have been further tailored by doping it with various metallic ions, such as Ag⁺, Au⁺, Mn⁺, Cu⁺,^{10,11} etc., or by conjugating it with other semiconductors like CdSe and CdS.^{12,13} The emission intensity is reported to be enhanced by doping with Ag⁺ which is termed as silver activated emission.¹⁴

These ZnS nanostructures with high luminescence emission have been shown to be synthesized by employing different methods such as doping^{14,15} and creation of Zn or sulfur vacancies.¹⁶ Recently, many articles suggesting the formation of green emitting ZnS nanostructures have been reported. The emission at around 525 nm is generally related to the charge carrier recombination from energy bands related to sulfur vacancies to the surface defects in ZnS.¹⁷ Doping of ZnS with Cu⁺, Mn⁺,

^{a)}Address all correspondence to this author.

e-mail: shash@barc.gov.in

DOI: 10.1557/jmr.2018.358

or other rare earth ions also lead to emission in the green region and is attributed to varying doping levels.¹⁸ However, the green emission around 538 nm for pure ZnS nanotubes was assigned to vacancy states and defect sites.⁷ Emission from pure ZnS nanobelts at 535 nm has also been related to the presence of elemental sulfur on the surface of nanostructures.¹⁹

The present work focusses on the synthesis and structural and optical study of pure ZnS and ZnS(Ag) powder. ZnS powder was synthesized by a chemical hydrothermal route and annealed at two different temperatures of 750 and 950 °C. The structural and morphological properties of the obtained nanostructures were studied by X-ray diffraction (XRD) and scanning electron microscopy, respectively. X-ray photoelectron spectroscopy (XPS) measurements were performed to understand the doping state and to rule out the presence of impurities in the synthesized powder. Ultra Violet-Visible (UV-Vis) spectroscopy and Photoluminescence (PL) measurements were performed to study their optical properties at room temperature. Characteristic blue emission was observed for the pure ZnS. However, for ZnS(Ag), it was observed that with the change in the annealing temperature from 750 to 950 °C, the energy of emitted radiation varied from the blue to green region of visible light. This change in the emitted wavelength may be attributed to the creation of additional sulfide defect states, due to the incorporation of excess Ag⁺ ions in the ZnS lattice. This shows a method to tune the ZnS luminescence just by changing the annealing temperature as well as it gives us better understanding of the mechanism of emission in ZnS(Ag).

II. EXPERIMENTAL METHODS

A. Material synthesis

Pure ZnS and Ag doped ZnS were synthesized by hydrothermal route using a Teflon-lined stainless-steel autoclave with a capacity of 250 mL. All the chemicals were analytical grade and were used without any further purification. 10 mM of zinc acetate [Zn(CH₃COO)₂] and 30 mM thiourea [NH₂CSNH₂] were dissolved completely in 20 mL deionized (DI) water in separate beakers. Thiourea was used in this experiment as it is a better sulfur producing agent during hydrothermal synthesis as compared to other sulfur agents like Na₂S. The two solutions were further mixed together and added to 60 mL ethylenediamine (ED) with continuous stirring for 30 min. ED acts as a template for the growth of sheet-like structures of ZnS and does not play any other role in the synthesis process. For Ag doping, 0.2 mM AgNO₃ was added to the final solution. Then the mixture was transferred to the autoclave which was then sealed and heated at 220 °C for 12 h. After cooling to room temperature, ZnS in the form of white precipitate was observed. The resulting precipitate was then separated from the solution using a centrifuge and

washed repeatedly with DI water and ethanol using ultrasonication. A white colored precipitate was observed for the pure ZnS, while a blackish-brown colored precipitate was obtained for the Ag doped ZnS. The products were further dried in air to obtain pure ZnS and Ag doped ZnS powders. The blackish-brown appearance of the Ag-doped ZnS powder may be due to the formation of the secondary Ag₂S phase. The as synthesized powder was later annealed in a vacuum (of the order of 5 × 10⁻⁵ mbar) at 750 and 950 °C for 10 h.

B. Characterization techniques

The phase purity of the synthesized powder samples was evaluated using X-ray diffractometer (Rigaku Model: RINT 2000 Dmax, Cu K_α line, Rigaku, Tokyo, Japan). A Carl Zeiss-Auriga field emission scanning electron microscope (FESEM) system (Carl Zeiss, Oberkochen, Germany) was used to study the morphology of the so obtained structures. PL studies were performed over a wavelength range from 200 to 800 nm by employing an Edinburg fluorescence spectrometer (model FLP920) in reflection geometry by positioning the samples at 45° with respect to the excitation beam. A xenon lamp was used as the excitation source, and a spectral bandwidth of 0.5 nm was selected for both excitation and emission monochromators. All the recorded luminescence spectra were corrected for the spectral sensitivity function of the instrument. The absorption spectra were recorded using a Shimadzu UV3600 spectrophotometer (Shimadzu, Kyoto, Japan). Ex situ XPS analysis on the sample was performed using a VG make model CLAM-2 hemispherical analyzer with the Mg K_α source (1253.6 eV) having a step size of 0.1 eV. The chamber pressure was maintained at 1 × 10⁻⁹ torr. Detailed fine scans were taken with pass energy 50 eV.

III. RESULTS AND DISCUSSION

A. Structural characterization

XRD measurements were performed on both pure ZnS and ZnS(Ag) powder before and after annealing. Figure 1 shows the respective powder XRD profiles of pure ZnS and ZnS(Ag) before and after annealing at 950 °C. The peak positions reveal the presence of both wurtzite and sphalerite crystal structures in ZnS powder with wurtzite as the dominating phase. All the observed peaks are identified for the ZnS wurtzite structure [JCPDS # 361450: $a = 3.82 \text{ \AA}$, $c = 6.257 \text{ \AA}$] and the peaks corresponding to the cubic sphalerite structure [JCPDS # 020565: $a = 5.400 \text{ \AA}$] are marked with asterisks in Fig. 1. The peak positions remain unaltered for both pure ZnS and ZnS(Ag) which ensure that no lattice distortion was introduced due to Ag doping. The FWHM of the XRD peaks was observed to decrease with annealing of the

powder due to an increase in grain-size. Hence the crystalline nature of the synthesized powder was observed to be enhanced with annealing. The size was estimated using Scherrer's formula

$$d = \frac{K\lambda}{\beta \cos(2\Theta/2)} ,$$

where d is the particle size, K is the constant close to unity, λ is the X-ray wavelength, β is FWHM of the XRD peak, and 2Θ is the peak position. The size of as-synthesized pure ZnS and ZnS(Ag) were observed to be around 52 nm and 31 nm, respectively. The particle sizes were observed to increase after annealing (at 950 °C) to around 58 and 67 nm for pure ZnS and ZnS(Ag) nanoparticles, respectively. The particle size was further confirmed using the TEM micrographs of the as prepared ZnS(Ag) powder given in Fig. 1(b). The particles are found to be spherical in shape and highly agglomerated with average size in the range of 50 nm similar to that calculated using XRD data.

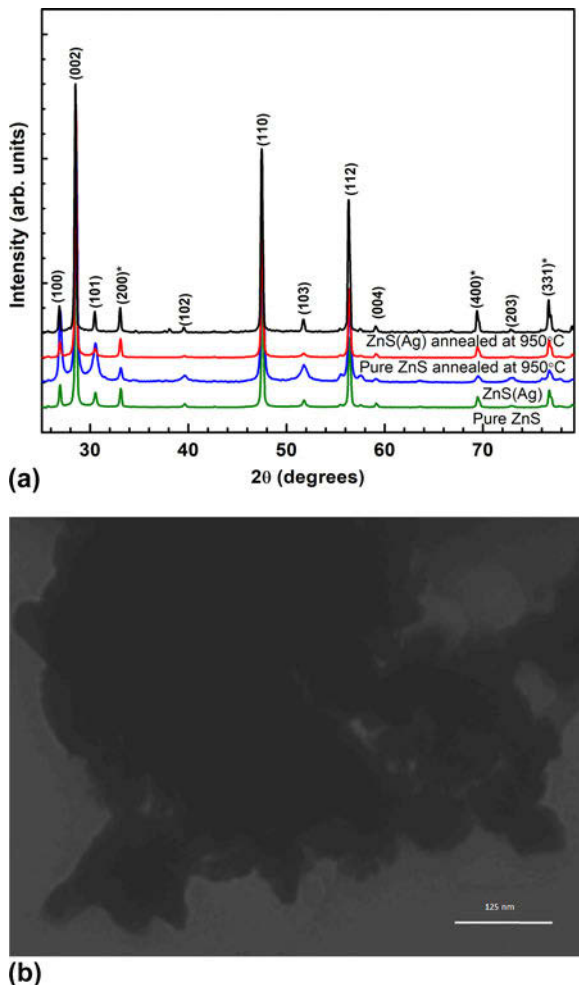


FIG. 1. (a) XRD profile of the pure ZnS and ZnS(Ag) nanoparticles with and without annealing at 950 °C in a vacuum. (b) TEM micrograph of the as synthesized ZnS(Ag) powder.

Figure 2 shows the FESEM images of as synthesized pure ZnS [Fig. 2(a)], pure ZnS annealed at 950 °C [Fig. 2(b)], and ZnS(Ag) nanoparticles after annealing at 950 °C [Fig. 2(c)]. Agglomerates of pure ZnS and ZnS(Ag) nanoparticles were observed whose size increased with annealing at 950 °C. The typical particle size of the agglomerated as-synthesized pure ZnS was observed to be around 300–500 nm and that of the agglomerates of annealed ZnS was seen to be around 2–3 μm. The particle size of both pure ZnS and ZnS(Ag) after annealing was observed to be approximately the same. This indicates that Ag doping does not alter the morphology of the ZnS powder. We see that the agglomerated particles have a plate-like structure with multiple plates stacking together. The growth of the plate-like structure occurs due to the presence of ED in the initial solution.²⁰

B. XPS characterization

To check the chemical purity of the synthesized ZnS powder and the presence of Ag in ZnS, XPS measurements were performed on the ZnS(Ag) samples annealed at 950 °C and the results are shown in Fig. 3. The XPS survey scan in Fig. 3(a) shows the presence of Zn, S, O, C, and a trace amount of Ag. The C 1s peak at 284.6 eV was used as the reference peak. This is the adventitious carbon peak which arises because of the presence of carbon in the ambient. The XPS spectra confirms the absence of impurities such as Cu, Mn, Mg, etc., in the ZnS(Ag) system.

S 2p peak [Fig. 3(b)] observed at 161.3 eV confirms the presence of sulfur in sulfide (S⁻) form.²¹ The absence of any elemental or oxidized form of sulfur was confirmed by the nonoccurrence of any additional peak from 163 to 170 eV.¹⁴ In the same figure, a strong peak at 139.16 eV can be observed, which corresponds to the Zn²⁺ 3s binding energy. This indicates the presence of interstitial Zn²⁺ defect sites in the sample which may be caused due to the presence of sulfur vacancies. The characteristic Zn 2p_{3/2} and 2p_{1/2} peaks at 1023 eV and 1046 eV, respectively, shown in Fig. 3(c) indicate the presence of Zn in 2⁺ states. The spin-orbit splitting of Zn 2p_{3/2} and 2p_{1/2} is 23 eV which corresponds to ZnS.²⁰ Relatively weak peaks at 368 and 374 eV were also observed as shown in the Fig. 3(d) which correspond to the Ag 3d_{5/2} and Ag 3d_{3/2} binding energy, respectively, which is characteristic of Ag⁺ in the Ag₂S product.^{22,23} In XRD, no peak corresponding to Ag₂S was observed as the amount is less than the detection limit of XRD.

C. UV-Vis spectroscopy

Figure 4(a) shows the UV-vis absorbance spectra of the pure ZnS and ZnS(Ag). The absorption of ZnS powder is found to increase on Ag doping as well as

on annealing for wavelengths higher than 350 nm. This can be due to the introduction of defect states in the ZnS lattice due to annealing under vacuum conditions. The absorption edge of all the samples was observed at 340 nm (3.64 eV) which is less than the band gap value

of bulk ZnS (3.72 eV). The absorption edges of the annealed samples show gradual fall as compared to the as-synthesized pure ZnS nanostructures which may be due to the formation of new defect states arising from annealing.

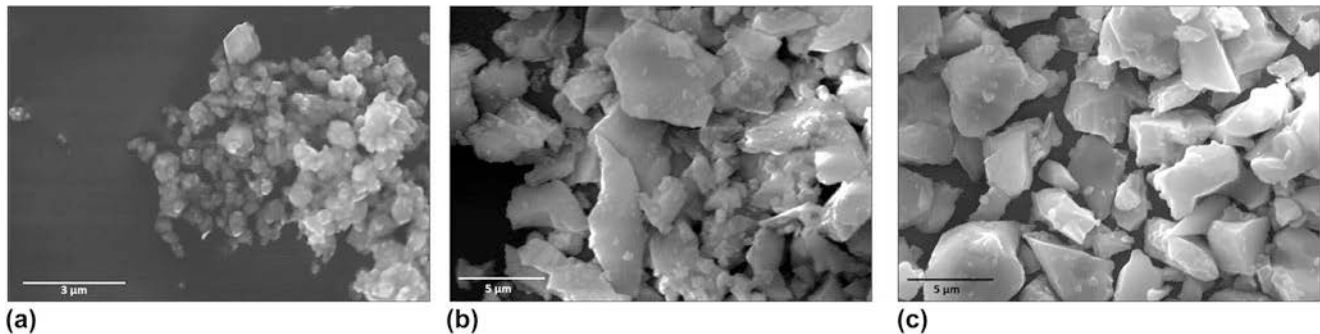


FIG. 2. SEM results of the ZnS nanoparticles: (a) pure ZnS nanoparticles, (b) pure ZnS nanoparticles after annealing at 950 °C, and (c) Ag doped ZnS nanoparticles after annealing at 950 °C.

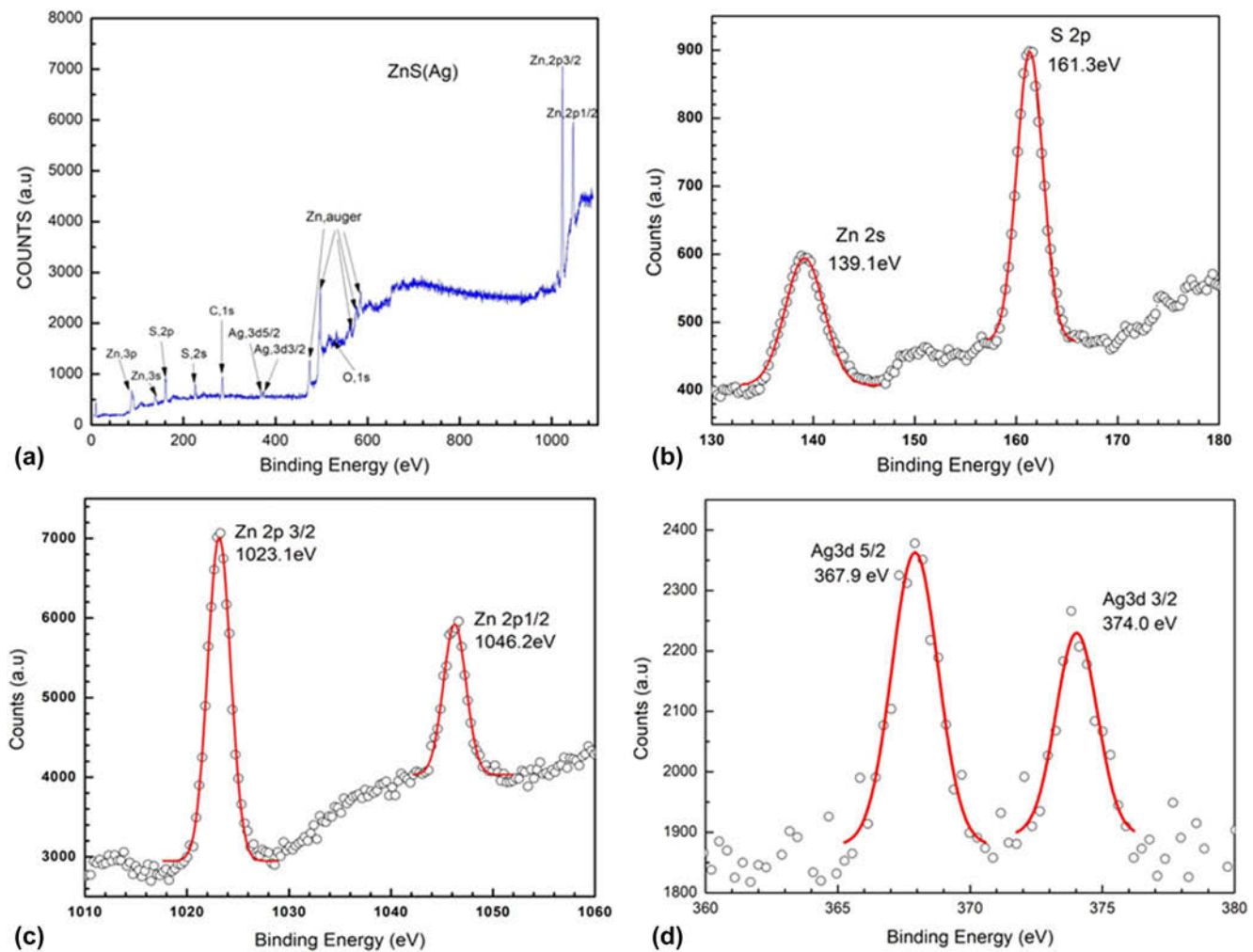


FIG. 3. (a) XPS survey spectrum of the Ag doped ZnS nanoparticles. (b), (c), and (d) represent the detailed XPS spectra of sulfur 2p, zinc 3s, zinc 2p, and silver 3d, respectively.

The absorption coefficient α is related to the optical band-gap E_g through the following relation:

$$\alpha h\nu = A(h\nu - E_g)^n ,$$

where $h\nu$ is the photon energy, A is proportionality constant, and n is a constant which may take values 1/2, 2, 3/2, and 3 depending upon the transition being allowed direct, allowed indirect, forbidden direct, and forbidden indirect, respectively. ZnS is a direct band-gap semiconductor, and the value of n for this system is 1/2.

Figure 4(b) shows the dependence of the optical absorption coefficient for different samples with photon energy. By extrapolating the linear portion of the Tauc plot to $\alpha = 0$, the band gap of pure ZnS and ZnS(Ag) nanostructures was observed as follows: 3.63 eV for pure and as synthesized ZnS, 3.54 eV for 950 °C annealed pure ZnS, 3.50 eV for ZnS(Ag) vacuum annealed at 750 °C, and 3.46 eV for ZnS(Ag) vacuum annealed at 950 °C. The vacuum annealing is found to decrease the estimated band gaps in these ZnS nanostructures. This is the manifestation of the presence of defect states created due to annealing and indirect transitions occurring in these particles. We would like to state that the increase in particle size on annealing will not have any effect on the band gap of the material because the particle size in our experiment is larger than what is required to show quantum confinement effects. The change in band gap due to the change in particle size is generally observed in particles with size in the range of 2–20 nm. Our particle size is in the range of 30 nm and above as confirmed by TEM and XRD results. Further investigations were carried out by studying the PL spectra of these materials.

D. PL spectroscopy

The PL spectra of pure ZnS nanoparticles vacuum annealed at 750 and 950 °C in a vacuum are shown in Fig. 5(a). The PL emission peaks were observed at

445 nm and 455 nm for the pure ZnS nanoparticles annealed at 750 °C and 950 °C, respectively. These emission peaks can be attributed to the transition from the sulfur vacancy state to the valance band edge. The sulfur vacancy states increase with the rise in annealing temperature from 750 to 950 °C leading to an increase in the intensity of the PL emission peak as can be seen in Fig. 5(a). Earlier, the emission in the blue region has been attributed to the transitions involving vacancy states in ZnS nanocrystals.¹⁰ As mentioned earlier, the possible defects in the ZnS lattice are Zn, S vacancies and Zn, S interstitial. The donor defects are sulfur vacancies and interstitial zinc atoms, while the acceptor defects are zinc vacancies and interstitial sulfur.²⁴ The energy states due to interstitial sulfur are located closer to the valence band edge (VBE) than the interstitial Zn to the conduction band edge (CBE). Similarly, the sulfur vacancy states are located closer to the conduction band than zinc vacancies to the valance band edge.²⁵ Emission at around 450 nm has also been observed previously in ZnS nanobelts²⁶ and nanowires and was attributed to either defect states or surface states.²⁷ Figure 5(b) shows the PL excitation (PLE) spectra for pure ZnS annealed at 750 °C and 950 °C. The PLE peaks observed at 337 nm and 339 nm for pure ZnS nanoparticles annealed at 750 °C and 950 °C, respectively, correspond to the band gap energy of ZnS²⁸ which was also observed in the UV-vis data analysis as shown in Sec. III.C. The energy band diagram representing the various possible transitions in pure ZnS are shown in Fig. 7(a).

For ZnS(Ag) powder annealed at 750 °C and 950 °C, the PL and PLE spectra are shown in Figs. 6(a) and 6(b), respectively. It can be clearly seen that the ZnS(Ag) powder annealed at 750 °C shows PL emission at 451 nm which is characteristic of ZnS(Ag) powder. During the hydrothermal synthesis of ZnS(Ag), Ag⁺ ions get incorporated into the ZnS lattice as a dopant and form Ag⁺ trap centers near the VBE. Thus, the emission at 451 nm

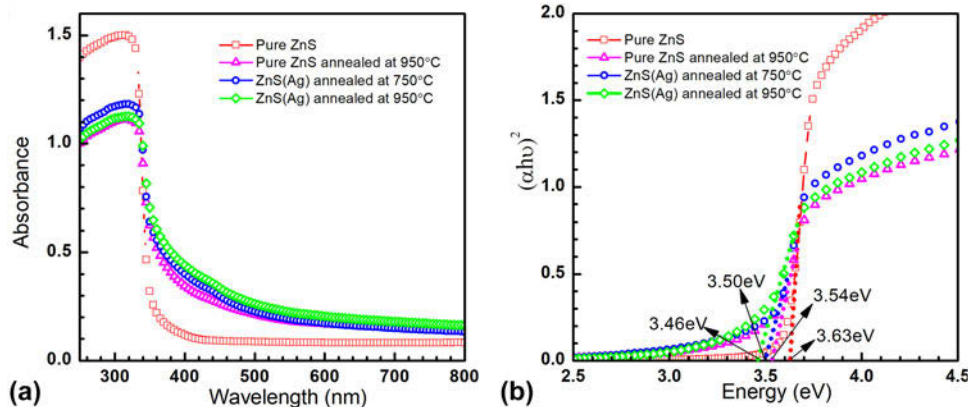


FIG. 4. (a) UV-vis absorbance spectra of the as synthesized ZnS and ZnS(Ag) nanoparticles annealed at 950 °C. (b) The Tauc plot of the given samples showing band-gap energies.

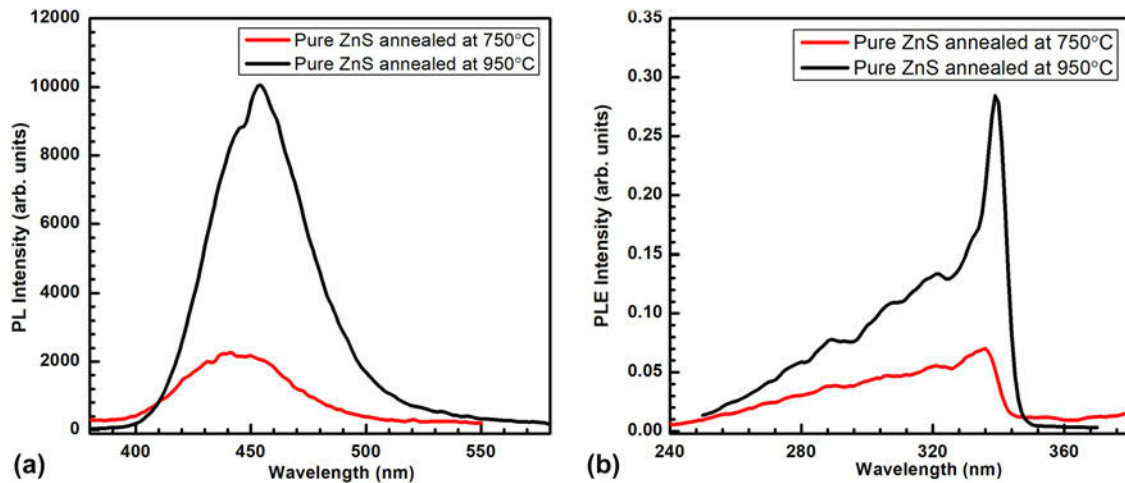


FIG. 5. The PL emission (a) and excitation (b) spectra of the pure ZnS nanoparticles annealed at 750 and 950 °C.

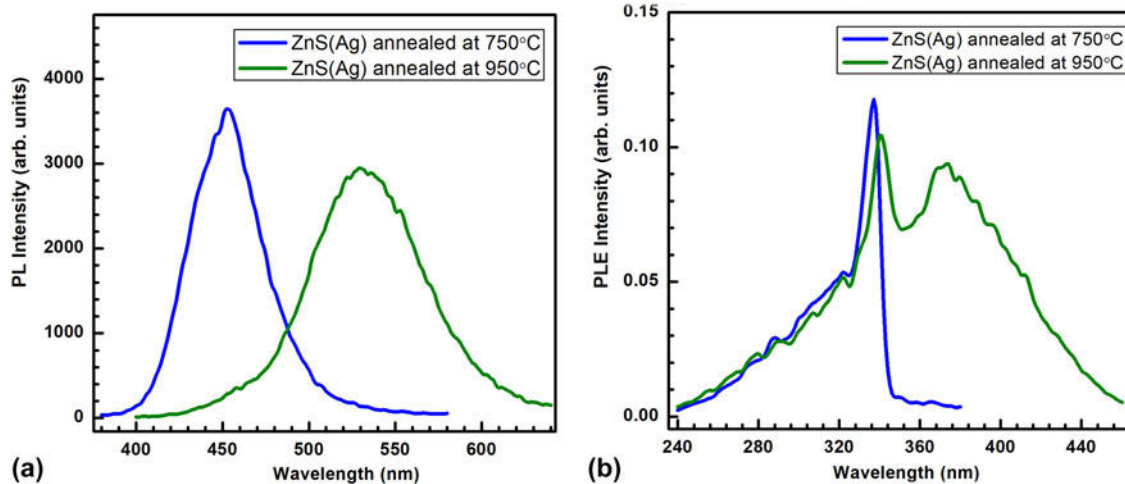


FIG. 6. PL emission (a) and excitation (b) spectra of ZnS(Ag) nanoparticles annealed at 750 and 950 °C.

arises from the radiative recombination of charge carriers from the CBE to Ag^+ states present near the VBE. For the ZnS(Ag) nanoparticles annealed at 950 °C, the PL emission peak was observed at 533 nm. Earlier, the green emission has been attributed to the presence of elemental S species on the surface of ZnS nanostructures.¹⁹ However, the presence of elemental sulfur in the present ZnS(Ag) nanostructures has been ruled out by the XPS studies as discussed in Sec. III.B.

The PLE spectra for ZnS(Ag) nanoparticles annealed at 750 and 950 °C show clear peaks around 340 nm corresponding to the ZnS energy band gap. Apart from that, another peak at 370 nm was observed for ZnS(Ag) nanoparticles annealed at 950 °C. This lower energy excitation suggests the presence of defect sites in the ZnS lattice which act as a metastable state and allow the absorption of photons corresponding to this energy. The excitation peak at 370 nm in Fig. 6(b) corresponds to the excitation of electrons from the VBE to the zinc interstitials present and the 340 nm excitation is related to

the CBE. In the case of pure ZnS samples, no excitation band around 370 nm was observed which indicates that the zinc interstitials in pure ZnS are very less and increase on Ag doping. These defect sites allow further relaxation of carriers to lower sulfide sites and final recombination at the Ag^+ centers giving rise to green PL emission at 533 nm. The energy band diagram depicting the various transitions is shown in Fig. 7(b).

A possible reason for higher sulfur vacancy in Ag doped ZnS can be that on annealing of ZnS(Ag) nanoparticles at 950 °C, which is a temperature higher than the melting point of Ag_2S (875 °C), more of Ag_2S dissociate and Ag^+ ions are incorporated in the ZnS lattice creating higher sulfur vacancies and zinc interstitials. These zinc interstitials act as trap centers for the electrons which are excited from the VBE. The trapped electrons may move onto the lower S vacancy states and finally recombine radiatively with the holes present at Ag^+ centers giving rise to green luminescence at 533 nm. The probability of nonradiative recombination within the S vacancy defect

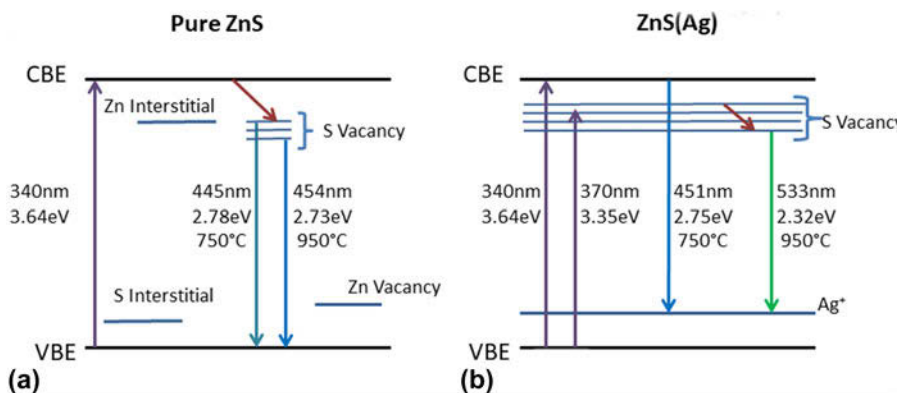


FIG. 7. Energy-band diagram showing the various optical transitions for (a) pure ZnS nanoparticles after annealing at 750 and 950 °C. (b) ZnS(Ag) nanoparticles after annealing at 750 and 950 °C.

sites lead to lower intensity of the 533 nm peak as compared to the 451 nm PL emission peak.

IV. CONCLUSION

Pure ZnS and ZnS(Ag) nanoparticles were synthesized by a template mediated simple hydrothermal route, and their vacuum annealing was performed at 750 and 950 °C.

It was observed that the annealing of pure ZnS nanoparticles at 750 and 950 °C gives rise to radiative transitions related mainly to the S vacancies present in the ZnS lattice. The luminescence emission from these pure ZnS nanoparticles has been observed in the blue region of the visible light. It has been shown that the emission wavelength from the ZnS(Ag) nanoparticles can be easily tuned from the blue to green region of visible light by changing the vacuum annealing temperature from 750 to 950 °C. This was found to be attributed to the formation of excess sulfur vacancies in ZnS on annealing at 950 °C under vacuum conditions. These additional sulfur vacancies arise due to the incorporation of further Ag⁺ ions in the ZnS lattice. This study provides a very simplified technique to synthesize ZnS(Ag) nanoparticles having optical emission in the green region. Such nanoparticles find huge application in imaging screens and can be easily integrated with the silicon photodiodes which show maximum sensitivity around 550 nm.

ACKNOWLEDGMENTS

The authors would like to thank GAMD, BARC for SEM measurements. M. Sharma would like to thank DST for INSPIRE Faculty grant.

REFERENCES

1. P. Sungsoon, A. Soyeon, K. Hyunsung, S. Lee, and C. Lee: Synthesis, structure and UV-enhanced gas sensing properties of Au-functionalized ZnS nano-wires. *Sens. Actuators, B* **188**, 1270–1276 (2013).
2. A.K. Kole, C.S. Tiwary, and P. Kumbhakar: Morphology controlled synthesis of wurtzite ZnS nanostructures through simple hydrothermal method and observation of white light emission from ZnO obtained by annealing the synthesized ZnS nano-structures. *J. Mater. Chem. C* **2**, 4338 (2014).
3. S.S. Boxi and S. Paria: Effect of silver doping on TiO₂, CdS, and ZnS nanoparticles for the photocatalytic degradation of metronidazole under visible light. *RSC Adv.* **4**, 37752 (2014).
4. Y. Liang, H. Liang, X. Xiao, and S. Hark: The epitaxial growth of ZnS nanowire arrays and their applications in UV-light detection. *J. Mater. Chem.* **22**, 1199–1205 (2012).
5. J.S. McCloy, M. Bliss, B. Miller, Z. Wang, and S. Stave: Scintillation and luminescence in transparent colorless single and polycrystalline bulk ceramic ZnS. *J. Lumin.* **157**, 416–423 (2015).
6. X. Fang, T. Zhai, U.K. Gautam, L. Li, L. Wu, Y. Bando, and D. Golberg: ZnS nanostructures: From synthesis to applications. *Prog. Mater. Sci.* **56**, 175–287 (2011).
7. Z. Li, B. Liu, X. Li, S. Yu, L. Wang, Y. Hou, Y. Zou, M. Yao, Q. Li, B. Zou, G. Zou, G. Wang, and Y. Liu: Synthesis of ZnS nanocrystals with controllable structure and morphology and their photoluminescence property. *Nanotechnol.* **18**, 255602 (2007).
8. R. Mendil, Z.B. Ayadi, and K. Djessas: Effect of solvent medium on the structural, morphological and optical properties of ZnS nanoparticles synthesized by solvothermal route. *J. Alloys Compd.* **678**, 87–92 (2016).
9. B.Y. Geng, X.W. Liu, Q.B. Du, X.W. Wei, and L.D. Zhang: Structure and optical properties of periodically twinned ZnS nanowires. *Appl. Phys. Lett.* **88**, 163104 (2006).
10. N. Murase, R. Jagannathan, Y. Kanematsu, M. Watanabe, A. Kurita, K. Hirata, T. Yazawa, and T. Kushida: Fluorescence and EPR characteristics of Mn²⁺-doped ZnS nanocrystals prepared by aqueous colloidal method. *J. Phys. Chem. B* **103**, 754 (1999).
11. K.B. Lin and Y.H. Su: Photoluminescence of Cu:ZnS, Ag:ZnS, and Au:ZnS nanoparticles applied in Bio-LED. *Appl. Phys. B* **113**, 351–359 (2013).
12. L. Lu, W. Zeng, S. Hu, D. Chen, J. Lei, and N. Ren: Polarization-dependent fluorescence of CdSe/ZnS quantum dots coupling to a single gold-silver alloy nanotube. *J. Alloys Compd.* **731**, 753–759 (2017).
13. X.J. Xu, L.F. Hu, N. Gao, S. Liu, S. Wageh, A.A. Al-Ghamdi, A. Alshahri, and X. Fang: Controlled growth from ZnS nanoparticles to ZnS-CdS nanoparticle hybrids with enhanced photoactivity. *Adv. Funct. Mater.* **25**, 445–454 (2015).

14. E. Hao, Y. Sun, B. Yang, X. Zhang, J. Liu, and J. Shen: Synthesis and photophysical properties of ZnS colloidal particles doped with silver. *J. Colloid Interface Sci.* **204**, 369–373 (1998).
15. Q. Pan, D. Yang, Y. Zhao, Z. Ma, G. Dong, and J. Qiu: Facile hydrothermal synthesis of Mn doped ZnS nanocrystals and luminescence properties investigations. *J. Alloys Compd.* **579**, 300–304 (2013).
16. J-C. Lee and D-H. Park: Self-defects properties of ZnS with sintering temperature. *Mater. Lett.* **57**, 2872–2878 (2003).
17. W. Zhang, X. Zeng, H. Liu, and J. Lu: Synthesis and investigation of blue and green emissions of ZnS ceramics. *J. Lumin.* **134**, 498–503 (2013).
18. P. Yang, M. Lu, D. Xu, D.L. Yuan, and G.J. Zhou: Photoluminescence properties of ZnS nanoparticles co-doped with Pb²⁺ and Cu²⁺. *Chem. Phys. Lett.* **336**, 76–80 (2001).
19. C. Ye, X. Fang, G. Li, and L. Zhang: Origin of the green photoluminescence from zinc sulfide nanobelts. *Appl. Phys. Lett.* **85**, 3035–3037 (2004).
20. S.A. Acharya, N. Maheshwari, L. Tatikondewar, A. Kshirsagar, and S.K. Kulkarni: Ethylenediamine-mediated wurtzite phase formation in ZnS. *Cryst. Growth Des.* **13**, 1369–1376 (2013).
21. M. Fantauzzi, B. Elsener, D. Atzei, A. Rigoldiab, and A. Rossiab: Exploiting XPS for the identification of sulfides and polysulfides. *RSC Adv.* **5**, 75953–75963 (2015).
22. G. Hota, S.B. Idage, and K.C. Khilar: Characterization of nano-sized CdS–Ag₂S core-shell nanoparticles using XPS technique. *Colloids Surf., A* **293**, 5–12 (2007).
23. S. Pan, X. Liu, and X. Wang: Preparation of Ag₂S–Graphene nanocomposite from a single source precursor and its surface-enhanced Raman scattering and photoluminescent activity. *Mater. Charact.* **62**, 1094–1101 (2011).
24. W. Becker and A.J. Bard: Photoluminescence and photoinduced oxygen adsorption of colloidal Zinc Sulfide dispersions. *J. Phys. Chem.* **87**, 4888–4893 (1983).
25. D. Denzler, M. Olschewski, and K. Sattler: Luminescence studies of localized gap states in colloidal ZnS nanocrystals. *J. Appl. Phys.* **84**, 2841–2845 (1998).
26. W.Q. Peng, G.W. Cong, S.C. Qu, and Z.G. Wang: Synthesis and photoluminescence of ZnS:Cu nanoparticles. *Opt. Mater.* **29**, 313–317 (2006).
27. Q. Xiong, G. Chen, J.D. Acord, X. Liu, J.J. Zengel, H.R. Gutierrez, J.M. Redwing, L.C. Lew Yan Voon, B. Lassen, and P.C. Eklund: Optical properties of rectangular cross-sectional ZnS nanowires. *Nano Lett.* **4**, 1663–1668 (2004).
28. S. Kakarndee, S. Juabrum, and S. Nanan: Low temperature synthesis, characterization and photoluminescence study of plate-like ZnS. *Mater. Lett.* **164**, 198–201 (2016).